

## Hydrodynamic interactions in ribbon channels: From quasi-one-dimensional to quasi-two-dimensional behavior

Sergey Novikov,<sup>1</sup> Stuart A. Rice,<sup>1</sup> Bianxiao Cui,<sup>2</sup> Haim Diamant,<sup>3</sup> and Binhua Lin<sup>4</sup>

<sup>1</sup>*Department of Chemistry and The James Franck Institute, The University of Chicago, Chicago, Illinois 60637, USA*

<sup>2</sup>*Department of Chemistry, Stanford University, Stanford, California 94305, USA*

<sup>3</sup>*School of Chemistry, Tel Aviv University, Tel Aviv 69978, Israel*

<sup>4</sup>*The James Franck Institute and Center for Advanced Radiation Sources, The University of Chicago, Chicago, Illinois 60637, USA*  
(Received 28 June 2010; revised manuscript received 13 August 2010; published 10 September 2010)

We present a study of the dynamics of confined suspensions whose dimensionality is intermediate between quasi-one-dimensional and quasi-two-dimensional (q2D) using microfluidic channels of various widths. The crossover between the two limiting behaviors is found to occur to different extent for different dynamic correlations between a pair of particles. In particular, the transverse coupling diffusion coefficient of particle pairs significantly deviates from its q2D form even in surprisingly wide channels.

DOI: [10.1103/PhysRevE.82.031403](https://doi.org/10.1103/PhysRevE.82.031403)

PACS number(s): 83.80.Hj, 47.60.Dx, 82.70.Dd

### I. INTRODUCTION

The motions of particles in a suspension are coupled via hydrodynamic interaction, which dictates the behavior of the suspension in confined geometries [1]. Problems related to the dynamics of confined suspensions have attracted considerable interest in recent years, both due to their relevance to microfluidics and nanofluidics and to the new physical effects that have been discovered in such systems [1–12]. To date, research has been naturally focused on the ideal limits of quasi-one-dimensional (q1D) suspensions (a single file of particles moving along a linear channel [3,6,7]) and quasi-two-dimensional (q2D) suspensions (a single layer of particles moving between two surfaces [2,5] or in a free-standing liquid film [9]). However, these studies do not address questions such as: (1) When do such limiting cases of integer dimensions apply in practice (for example, in biological or microfluidic scenarios)? (2) Under what conditions can a confined suspension be regarded as q2D or q1D? In this paper we report the results of experimental and theoretical studies of hydrodynamic interaction in a colloid suspension confined in microfluidic channels of various width-to-depth aspect ratios, a system intermediate between q1D and q2D.

It is now widely appreciated that fluids restricted to have one-dimensional (1D) and two-dimensional (2D) geometries have unique properties, different from those in three dimensions, which can be traced to the character of the confinement [1]. In unconfined three-dimensional suspensions hydrodynamic interactions between particles are long ranged, have many-body contributions, and are positive (particles drag one another in the same direction) [13].

Consider a q1D colloid suspension confined in a narrow channel whose width  $w$  is less than  $2\sigma$  ( $\sigma$  is the diameter of a colloid particle). A capillary-Stokeslet analysis of the influence of hydrodynamic interactions on the pair-diffusion coefficients reveals that the interaction between particles decays exponentially with the particle separation  $r$ , and the screening length is proportional to  $w$  [3,14]. The capillary-Stokeslet approximation, which neglects the effects associated with the nonzero size of the colloid particles, does not

correctly describe the small separation ( $r \sim \sigma$ ) dependence of the pair-diffusion coefficient associated with the particle excluded volume; that behavior is correctly described when the influence of the nonzero size of the colloid particles on the fluid motion and the spatial correlation of particle positions are accounted for, as shown by Xu *et al.* [6].

Consider now a q2D colloid suspension confined between two hard walls with a small separation  $H$  ( $H \sim \sigma$ ). A Stokeslet hydrodynamic analysis shows that in such a system the far-field flow induced by the motion of a colloid particle has a momentum monopole contribution that is cut off by the boundary conditions at distances larger than the confinement spacing  $H$  and a mass dipole contribution that decays with pair separation as  $(H/r)^2$ , with the anisotropy of the dipolar flow field being responsible for the negative sign of the coupling that affects the transverse pair-diffusion coefficient [2,15]. It has also been demonstrated that the correction to the large-distance hydrodynamic pair interaction due to third particles (the first-order correction in colloid density) vanishes.

In Ref. [1], Stokeslet hydrodynamic analyses were used to derive different scaling relations for the dependence of the hydrodynamic coupling between particles on  $r$  and the confining length scales ( $w$  or  $H$ ) for various q1D and q2D geometries; the hydrodynamic interactions in q2D fluid membranes, in q2D free-standing liquid films, and in porous materials decay as  $1/r$ ,  $\ln(r)$ , and  $1/r^3$ , respectively. The experimental evidence supporting those scaling laws is cited in Ref. [1].

To date, none of the theoretical and experimental studies of q1D and q2D colloid equilibrium dynamics have focused attention on the transition between q1D and q2D behaviors, although there have been several studies of the changes in equilibrium packing structure associated with that transition [16,17] and a study of the driven motion of 1D microfluidic droplets at the crossover between 2D flow and 1D plug flow [7]. Here, we report measurements of the pair diffusion in one-layer deep colloid suspensions confined in ribbon channels with ribbon widths from 1 to 12 particle diameters and the comparisons of these results with the theoretical predictions. The separation dependence of the pair diffusion probes

the complex changes in hydrodynamic coupling that accompany the change in geometry, which lead to different asymptotic forms in q1D and q2D for the pair-diffusion coefficients. The current research follows up our earlier studies of the packing structure in q1D ribbon colloid suspensions as a function of ribbon width [18] and of hydrodynamic interactions in q1D and q2D colloid suspensions [2,3].

The structure of a confined fluid depends strongly on the geometry of the confinement. The salient feature of a q1D ribbon system is that the density distribution of the fluid transverse to the ribbon channel is stratified, and that the order along the strata is characteristic of a q1D liquid, even at a density near to close packing [18]. However, if the stratified density distribution is ignored we find that the order on the length scale of the width of the channel is characteristic of a q2D liquid or solid. These results suggest that ribbon suspensions fall into the unknown domain between q1D and q2D geometries, and that the behavior of the longitudinal and transverse pair-diffusion coefficients in ribbon-confined suspensions may have interesting information that is relevant to understanding the transition between q1D and q2D behaviors [18].

## II. EXPERIMENTAL DETAILS

Our experimental system consists of a sample cell that contains an aqueous suspension of silica spheres (Duke Scientific,  $\sigma = 1.58 \pm 0.04 \mu\text{m}$ , density of  $2.2 \text{ g/cm}^3$ ) confined to long narrow channels of various widths  $w$ , but the same depth  $h$  ( $h = 3 \mu\text{m}$ ) [18]. The length of these channels is 10 mm. The channels were printed on a polydimethylsiloxane (PDMS) substrate from a master pattern fabricated lithographically (Stanford Nanofabrication Facility). The colloid suspension was enclosed between the PDMS mold and a cover slip with a PDMS spacer of  $\sim 100 \mu\text{m}$ , so that the top of the channels was open to a layer of fluid. The colloid particles settled quickly into the channels gravitationally, floating near, but not touching, the bottom of the channels; the distance between the bottom of the particles and the bottom of the channel was measured previously to be about  $0.3 \mu\text{m}$  [19]. The vertical motion of the particles was very limited during the measurements. Care has been taken to assure that the channels were not blocked in the vicinity (around several hundreds of micrometers) of the field of view ( $108 \mu\text{m}$ ) where the images were captured. Previous studies in this laboratory have also established that the effective colloid-colloid interaction does not depend on the ionic strength of the suspension fluid, indicating that the contribution of the small residual charge on the silica spheres of the interaction of the spheres is negligible [20].

Digital video microscopy was used to extract time-dependent two-dimensional trajectories of the colloid particles (with a time resolution of 0.033 s). Figure 1 shows images of the colloid suspension confined in a channel ( $w = 20 \mu\text{m}$ ) at different packing fractions. We used the same video microscopy setup and data processing procedures that have been described in detail elsewhere [20]. Briefly, the images of the suspension were captured at 30 frames per second using a Hitachi charge-coupled device video camera

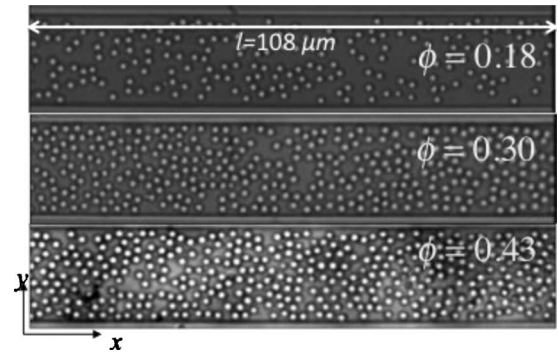


FIG. 1. Images of the colloid suspension confined in a ribbon channel ( $w = 20 \mu\text{m}$ ) at low, medium, and high packing fractions.

whose analog output was sent to a Sanyo GVR-S955 VCR. We used Scion Image software and a CG-7 frame grabber card (Scion Corporation) to digitize the sequence of the images, i.e., the “movies.” The maximum number of pixels in an image is  $640 \times 480$ , and the length-to-pixel ratio is  $0.169 \mu\text{m}/\text{pixel}$ . Image analysis techniques developed by Crocker and Grier [21] were used to locate the centers of the colloids with a precision of  $\sim 20 \text{ nm}$ .

Using histograms of the particle locations, we verified that the particle-density distributions in all samples were uniform along the  $x$  axis (the direction of the channel). However, the extent of particle trajectories transverse to the channel (the  $y$  axis) is less than expected in the absence of direct colloid-wall interaction other than excluded volume, which we attribute to the nonwetting property of the PDMS wall [18]. The effective width of the channel,  $w_{\text{eff}}$ , is approximately  $1 \mu\text{m}$  less than  $w$  along each wall, as calculated from the histogram of the colloid particle positions and the distance between the most widely separated density peaks; we assume, likewise, that the effective depth of all the channels is  $h_{\text{eff}} \approx 2 \mu\text{m}$ . For clarity, the experimental data sets will be referred to using the fabricated channel width  $w$ . The packing fraction was calculated using  $\phi = N\pi\sigma^2/4lw_{\text{eff}}$ , with  $l$  as the length of the channel in the field of view ( $108 \mu\text{m}$ ) and  $N$  as the average number of particles in the viewed section of the channel. For each channel width, measurements were taken at different packing fractions around three values: low ( $\phi \approx 0.18$ ), medium ( $\phi \approx 0.28$ ), and high ( $\phi \approx 0.43$ ).

The data for the q1D and q2D geometries [2,3] presented for comparison with our measurements were obtained using the same colloid preparation and the video microscopy setup; the width of the q1D channel was  $3 \mu\text{m}$ , and the gap between the two hard walls in the q2D cell was  $1.7 \mu\text{m}$ . The linear packing fraction  $\eta$  ( $\eta = N\sigma/l$ ) for the q1D data used is  $\eta = 0.17$ , and the packing fraction for the q2D data used is  $\phi = 0.25$ .

## III. RESULTS AND DISCUSSION

Our experiments focus attention on four questions relevant to the transition between q1D and q2D. First, given the stratification of the density distribution transverse to the ribbon channel, do the pair-diffusion coefficients within one stratum behave as if the particles were in a q1D channel, or

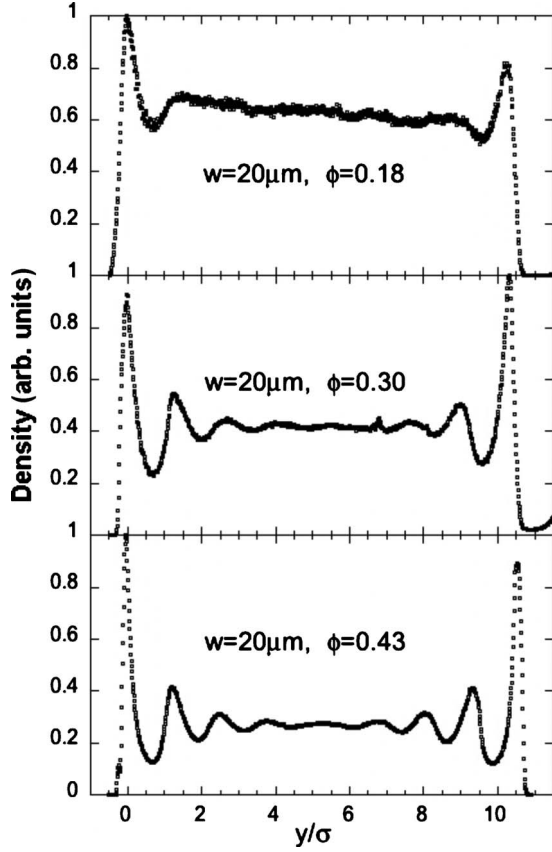


FIG. 2. Stratified transverse density distributions of the samples shown in Fig. 1. The asymmetry in the density distribution may arise from a slight tilt of the sample cell on the microscope stage, which is hard to discern from the images themselves [18].

does the corrugation of the nearest-neighboring strata generate different behaviors? Second, does the pair-diffusion coefficient vary from stratum to stratum across the channel? Third, if the stratification of the transverse density distribution in the ribbon channel is disregarded, how does the pair-diffusion coefficient for the confined suspension differ from that in an infinite q2D suspension? Finally, when the particle separation is comparable to and larger than the width of the channel, does the pair-diffusion coefficient averaged over the entire channel exhibit q1D character?

The stratification of the transverse density distribution of the colloid particles in a ribbon channel is evident even at very low packing fraction such as  $\phi \approx 0.18$  [18], as demonstrated in Fig. 2. We use the short-time pair-diffusion coefficients to compare the hydrodynamic interactions in stratum with those throughout the ribbon channel, because the predicted large pair separation behavior of these coefficients is different in q1D and q2D geometries. For particles in the same stratum, we examine both the longitudinal and transverse pair-diffusion coefficients, defined as

$$D_L^\pm(r) \equiv \left\langle \frac{[x'_1(t) \pm x'_2(t)]^2}{4t} \right\rangle_r = \frac{1}{4t} \sum_{i,j}^N \frac{[x'_i(t) \pm x'_j(t)]^2}{N^2} \quad (1)$$

$$\xrightarrow[r \rightarrow \infty]{} D_L^S,$$

$$D_T^\pm(r) \equiv \left\langle \frac{[y'_1(t) \pm y'_2(t)]^2}{4t} \right\rangle_r = \frac{1}{4t} \sum_{i,j}^N \frac{[y'_i(t) \pm y'_j(t)]^2}{N^2} \quad (2)$$

$$\xrightarrow[r \rightarrow \infty]{} D_T^S,$$

respectively, in which  $x'_1(t)$  and  $y'_1(t)$  are, respectively, the displacements  $[x'_1(t) = x'_1(t_2) - x'_1(t_1)]$  and  $[y'_1(t) = y'_1(t_2) - y'_1(t_1)]$  of particle 1 along ( $L$ ) and perpendicular ( $T$ ) to the line connecting it to particle 2 during a time interval  $t$  ( $t < 0.2$  s), and  $r$  is the separation between these two particles.

In the capillary-Stokeslet analysis, a reduced pair-diffusion coefficient is used; it is defined as

$$\Delta_{L,T}^\pm \equiv \frac{[D_{L,T}^\pm(\xi) - D_{L,T}^S]}{[(\sigma/2R)D_0]}, \quad \xi \equiv \frac{r}{R}, \quad (3)$$

with  $D_0 = k_B T / 3\pi\mu\sigma$ ,  $R$  as the effective radius of the capillary, and  $\mu$  as the shear viscosity of the solvent. It has been shown [3,14] that in a q1D channel the longitudinal pair-diffusion coefficients  $\Delta_x^\pm$ , taken along the channel axis ( $x$ -axis), for all packing fractions collapse onto the curve calculated from the capillary-Stokeslet analysis when they are rescaled using Eq. (3). We note that  $\Delta_L^\pm$  and  $\Delta_x^\pm$  for the q1D fluid are identical within the experimental precision; measurements of  $\Delta_T^\pm$  for a q1D fluid have not been reported before. For the q1D channel reported previously,  $2R = \gamma w$  (for  $w = 3 \mu\text{m}$  and  $\gamma \approx 2.44$ ).

We first focus on the measurements of  $D_{L,T}^\pm$  and  $\Delta_{L,T}^\pm$  in a single stratum, scaling  $\Delta_{L,T}^\pm$  using Eq. (3). Consider two of the ribbon channels ( $w = 8 \mu\text{m}$  and  $w = 20 \mu\text{m}$ ) at  $\phi \approx 0.18$ . Our data show that the values of  $D_{L,T}^\pm$  and  $D_{L,T}^S$  in the strata adjacent to the walls on each side of the channels are smaller than those in the interior strata (Fig. 3), as expected from the wall-drag effect [22]. However, when rescaled using Eq. (3), all of the data for the two channel widths shown in Fig. 3 as well as the data for the other channel widths at the lower packing fraction (Fig. 4), and for the medium and higher packing fractions (Figs. 5 and 6), fall on universal curves for  $\Delta_{L,T}^\pm$ , the same as those found in the q1D fluid [3], implying that many-body interactions are screened in this confined geometry.

Overall, the reduced pair-diffusion coefficients in stratum and the q1D capillary-Stokeslet approximation for the large separation behavior of  $\Delta_{L,T}^\pm$  are in good agreement, as shown in Figs. 4–6. The data for  $\Delta_L^\pm$  show the predicted exponential decay at large particle separation. The data for  $\Delta_T^\pm$  display steeper exponential decay at small particle separation than do the data for  $\Delta_L^\pm$ , in agreement with prediction [14], but not the predicted nonmonotonic decay at intermediate pair separation.

A further test of the consistency of the q1D capillary-Stokeslet approximation for large pair separation is provided by the lack of variation in the values of the effective radius  $R$ , which is required to fit the large separation behavior

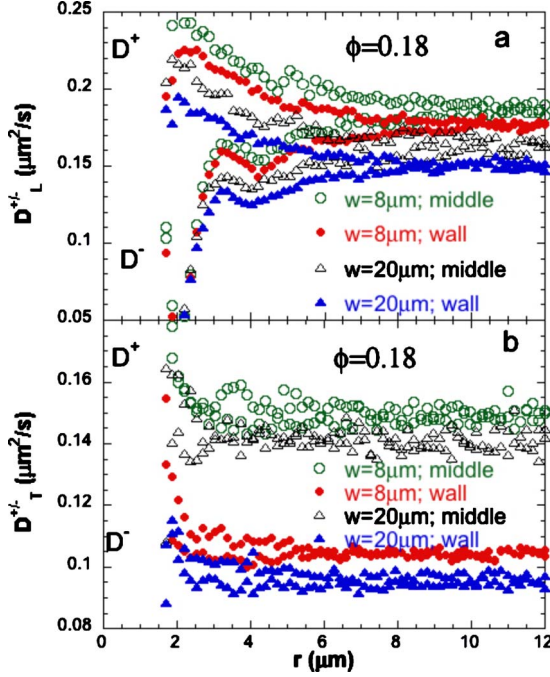


FIG. 3. (Color online) Typical in-stratum (a) longitudinal and (b) transverse pair-diffusion coefficients  $D_{L,T}^{\pm}$  of the particles in a stratum adjacent to a channel wall and those in a stratum in the middle of the channels.

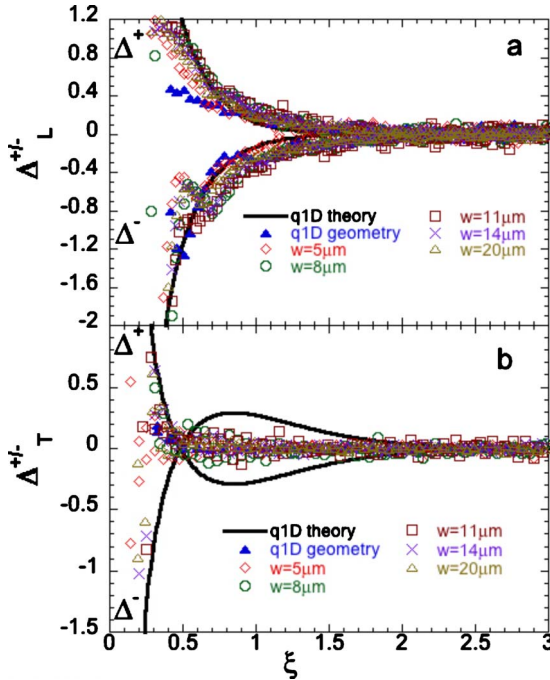


FIG. 4. (Color online) Reduced in-stratum (a) longitudinal and (b) transverse pair-diffusion coefficients  $\Delta_{L,T}^{\pm}$  of particles in the ribbon channels at low packing fraction ( $\phi \approx 0.18$ ). Each curve represents the average of  $\Delta_{L,T}^{\pm}$  for all of the strata in each ribbon, compared with that in a q1D fluid at  $\eta=0.17$  [3]. The lines are the predictions obtained from the q1D capillary-Stokeslet hydrodynamic analysis [14].

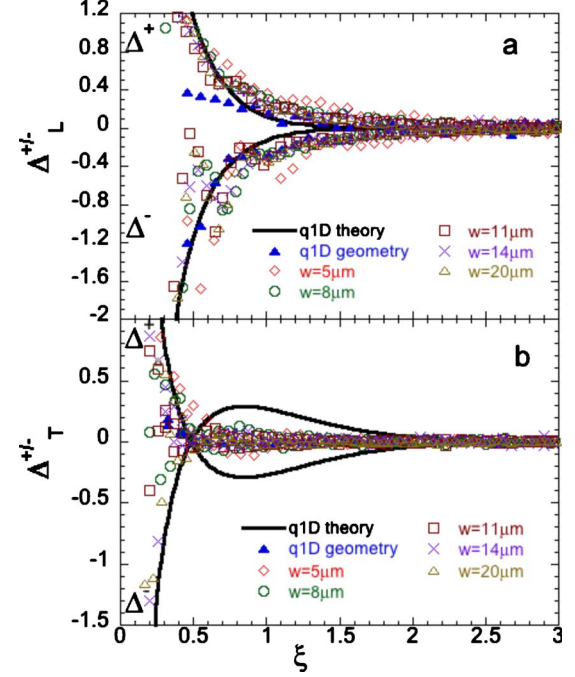


FIG. 5. (Color online) Reduced in-stratum (a) longitudinal and (b) transverse pair-diffusion coefficients  $\Delta_{L,T}^{\pm}$  of particles in the ribbon channels at medium packing fraction ( $\phi \approx 0.28$ ). Each curve represents the average of  $\Delta_{L,T}^{\pm}$  for all of the strata in each ribbon, compared with that in a q1D fluid at  $\eta=0.17$  [3]. The lines are the predictions obtained from the q1D capillary-Stokeslet hydrodynamic analysis [14].

of  $\Delta_{L,T}^{\pm}$  for each stratum. The value of the effective radius  $R$  for all the strata and packing fractions for channels with  $w > 5 \mu\text{m}$ , averaged over the values for several strata in each channel, is  $R \approx 6 \mu\text{m}$ , implying that  $R$  is sensibly related to the width of the strata,  $w_{st}$ , which is a constant (for  $w > 5 \mu\text{m}$ ,  $w_{st} = (1.25 \pm 0.05)\sigma$  [18]; hence,  $2R = \gamma w_{st} \approx 6.1 w_{st}$ ), but independent of  $w$  and  $\phi$ . For  $w = 5 \mu\text{m}$ ,  $w_{st} \approx \sigma$  and  $R \approx 4 \mu\text{m}$ . These results provide strong support for the argument that the colloid particles in a stratum behave as if in a q1D capillary. Additional support for this argument comes from the observation that the small separation behavior of  $\Delta_{L,T}^{\pm}$ , more pronounced at the higher packing fractions, mimics that in a q1D channel, with oscillations related to the small separation structure of the q1D pair correlation function [6].

Some information about the transition between q1D and q2D behaviors can be obtained from a comparison of  $\Delta_{L,T}^{\pm}$  for individual strata in a ribbon channel, described above, with that measured for particles across the whole channel, neglecting the stratification of the transverse density distribution, i.e., a pseudo-q2D analysis that characterizes the suspension in the ribbon channel only by  $\phi$ . In this analysis, the diffusion coefficients  $D_L^{\pm}(r)$  and  $D_T^{\pm}(r)$  are obtained from the trajectory data via the same definitions as used for the in-stratum pair-diffusion coefficient calculations, given in Eqs. (1) and (2). A rescaling similar to that used to reduce the q1D pair-diffusion data to a universal curve has been shown to

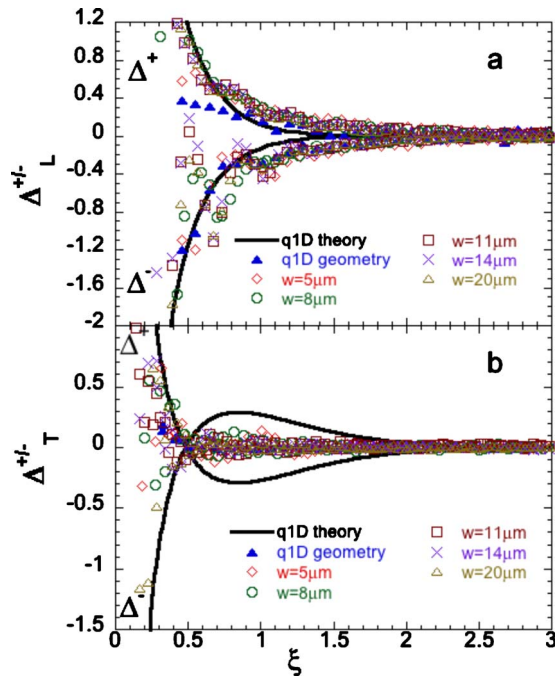


FIG. 6. (Color online) Reduced in-stratum (a) longitudinal and (b) transverse pair-diffusion coefficients  $\Delta_{L,T}^{\pm}$  of particles in the ribbon channels at high packing fraction ( $\phi \approx 0.43$ ). Each curve represents the average of  $\Delta_{L,T}^{\pm}$  for all of the strata in each ribbon, compared with that in a q1D fluid at  $\eta = 0.17$  [3]. The lines are the predictions obtained from the q1D capillary-Stokeslet hydrodynamic analysis [14].

rescale the q2D pair-diffusion coefficients to a universal curve [2]. This rescaling has the form

$$\Delta_{L,T}^{\pm} \equiv \frac{[D_{L,T}^{\pm}(\rho) - D_{L,T}^S]}{[(\sigma/2H)D_0]}, \quad \rho \equiv \frac{r}{H}, \quad (4)$$

where  $H$  is the gap between the two parallel walls in a q2D fluid [2].

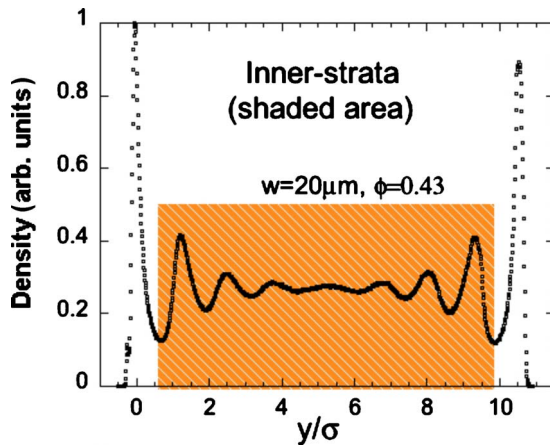


FIG. 7. (Color online) The shaded area defines the inner strata of a transverse particle-density distribution of the colloid suspension confined in a ribbon channel ( $w = 20 \mu\text{m}$ ). The calculations for the pseudo-q2D pair-diffusion coefficients include the particles only in those inner strata.

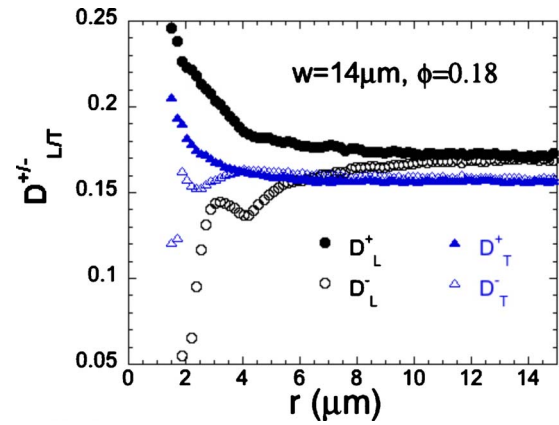


FIG. 8. (Color online) A typical set of pseudo-q2D  $D_{L,T}^{\pm}$  for the particles in the inner strata of the ribbon channels.

While our data reveal a significant influence of the wall-drag effect on the pseudo-q2D  $D_{L,T}^{\pm}$  (which will be described in a separate report), we focus here on the behavior of the q1D to q2D crossover by removing the particles that are in the two strata adjacent to the walls and considering only the inner-strata particles, as illustrated in Fig. 7 (except for the  $5 \mu\text{m}$  channel that holds only two strata). Figure 8 shows a typical set of pseudo-q2D  $D_{L,T}^{\pm}$  for the particles in the inner strata of the ribbon channels.

We now examine the rescaled pseudo-q2D pair-diffusion coefficients for  $r \leq w$  and for  $r \gg w$ , respectively, expecting

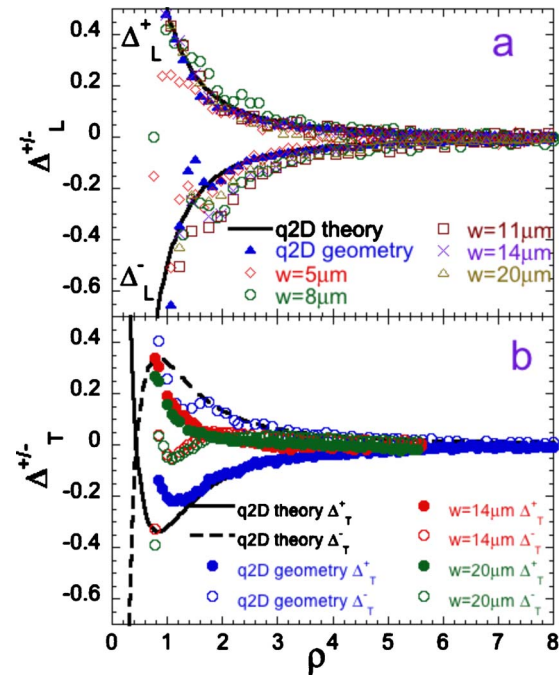


FIG. 9. (Color online) Reduced pseudo-q2D (a) longitudinal and (b) transverse pair-diffusion coefficients  $\Delta_{L,T}^{\pm}$  for the particles in the inner strata of the ribbon channels, scaled by a common factor  $H \approx 2.2 \mu\text{m}$ , at low packing fraction ( $\phi \approx 0.18$ ). For  $\Delta_T^{\pm}$ , only  $w = 14$  and  $20 \mu\text{m}$  are shown for clarity. Also displayed are  $\Delta_L^{\pm}$  and  $\Delta_T^{\pm}$ , respectively, for the q2D fluid at  $\phi = 0.25$  [2]. The lines are the predicted  $\Delta_{L,T}^{\pm}$  from the Stokeslet hydrodynamic analysis for a 2D geometry [15].

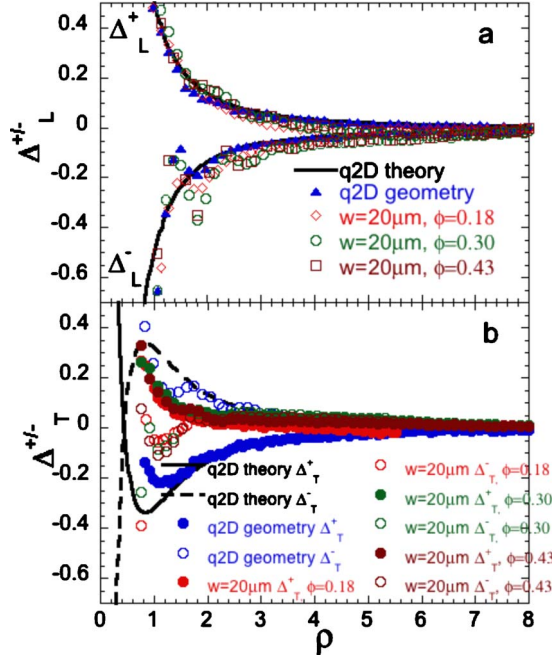


FIG. 10. (Color online) Reduced pseudo-q2D (a) longitudinal and (b) transverse pair-diffusion coefficients  $\Delta_{L,T}^{\pm}$  for the particles in the inner strata of a ribbon channel ( $w=20 \mu\text{m}$ ), scaled by a common factor  $H \approx 2.2 \mu\text{m}$ , at three packing fractions ( $\phi=0.18, 0.30$ , and  $0.43$ ). For  $\Delta_T^{\pm}$ , only  $w=14$  and  $20 \mu\text{m}$  are shown for clarity. Also displayed are  $\Delta_L^{\pm}$  and  $\Delta_T^{\pm}$ , respectively, for the q2D fluid at  $\phi=0.25$  [2]. The lines are the predicted  $\Delta_{L,T}^{\pm}$  from the Stokeslet hydrodynamic analysis for a 2D geometry [15].

that when  $r \leq w$  the system will exhibit q2D behavior, while for  $r \gg w$  the ribbon-channel may act as an effective q1D channel. Consider first the rescaled pseudo-q2D pair-diffusion coefficients  $\Delta_{L,T}^{\pm}$  calculated using Eq. (4) for  $r \leq w$  at the lower packing fraction ( $\phi \approx 0.18$ ). Figure 9(a) shows  $\Delta_L^{\pm}$ ; the value of  $H$  required to rescale these data is  $H \approx 2.2 \mu\text{m}$ , very close to the value of  $h_{eff}$ . It is readily seen that the pseudo-q2D  $\Delta_L^{\pm}$  for the particles in the inner strata follow the same behavior as does  $\Delta_L^{\pm}$  measured for the q2D liquid obtained previously [2] and are well described by

$$\Delta_L^{\pm}(\rho \gg 1) = \pm \lambda / \rho^2, \quad (5)$$

with  $\lambda=0.31$ , as derived from the Stokeslet hydrodynamic analysis for a 2D liquid [2]. The values of the pseudo-q2D  $\Delta_T^{\pm}$  of particles in the inner strata, rescaled by the same factor  $H$  used for the pseudo-q2D  $\Delta_L^{\pm}$ , are shown in Fig. 9(b); there are clear deviations from the expected q2D behavior in two respects: the pseudo-q2D  $\Delta_T^{\pm}$  do not have the reversed signs found for  $\Delta_T^{\pm}$  in the q2D case (in two dimensions,  $\Delta_T^{\pm}(\rho \gg 1) = \mp \lambda / \rho^2$ , with  $\lambda=0.31$  [2]), and the pseudo-q2D  $\Delta_T^{\pm}$  approach the large separation limit much faster than do the q2D  $\Delta_T^{\pm}$ . Thus, for  $r \leq w$  the transverse pair motion in the ribbon channel does pick up characteristic differences between q1D and q2D confinements and leads to the conclusion that those differences persist for the widest ribbon channels we have studied.

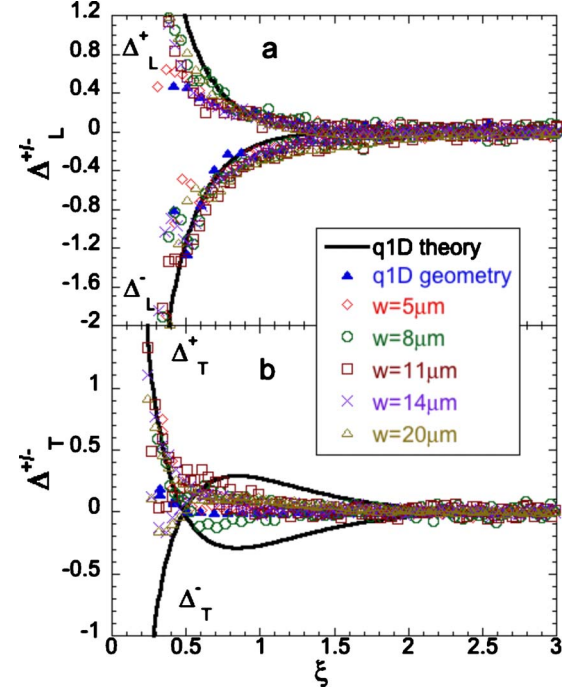


FIG. 11. (Color online) Reduced pseudo-q2D (a) longitudinal and (b) transverse pair-diffusion coefficients  $\Delta_{L,T}^{\pm}$  at low packing fraction ( $\phi \approx 0.18$ ) for the particles in the inner strata of a ribbon channel ( $w=20 \mu\text{m}$ ), scaled by a factor  $R$  ( $5 \leq R \leq 8 \mu\text{m}$ ). Also displayed are  $\Delta_{L,T}^{\pm}$  for the q1D fluid at  $\eta=0.17$  [3]. The lines are the predicted  $\Delta_{L,T}^{\pm}$  from the Stokeslet hydrodynamic analysis for a q1D geometry [14].

The behaviors of the pseudo-q2D  $\Delta_{L,T}^{\pm}$  described above are independent of the packing fraction, except for the more pronounced oscillations at the smaller separations. Figure 10 shows, as an example, the pseudo-q2D  $\Delta_{L,T}^{\pm}$  for one of the ribbon channels ( $w=20 \mu\text{m}$ ) at different packing fractions. As in the case of the q2D fluid, this density-independent behavior is indicative of the absence of many-body interaction at large distances [1,2,23].

The effect of the ribbon-channel confinement on the flow field when  $r \leq w$  is counterintuitive. It is reasonable to expect that, as the width of the channel becomes much larger than the particle diameter, the hydrodynamic interaction between the particles would decay as  $1/r^3$ , as predicted for a pair of spheres near one hard wall (the bottom of the channel in our case) [11]. However, the measured pseudo-q2D  $\Delta_L^{\pm}$  decays as  $1/r^2$ , the same as  $\Delta_L^{\pm}$  measured for a layer of particles confined tightly between two hard walls, as if the stratified monolayer of particles serves as an effective second wall parallel to the bottom of the channel. On the other hand, the channel walls appear to have destroyed the anisotropy of the dipolar flow field associated with the behavior of the pseudo-q2D  $\Delta_T^{\pm}$ , both quantitatively (in their magnitudes) and qualitatively (in their signs).

We now consider the rescaled pseudo-q2D pair-diffusion coefficients  $\Delta_{L,T}^{\pm}$  calculated using Eq. (3) for  $r \gg w$ . Figure 11 shows the rescaled pseudo-q2D  $\Delta_{L,T}^{\pm}$  for the lower packing fraction ( $\phi \approx 0.18$ ). The values of  $R$  required to fit the data to

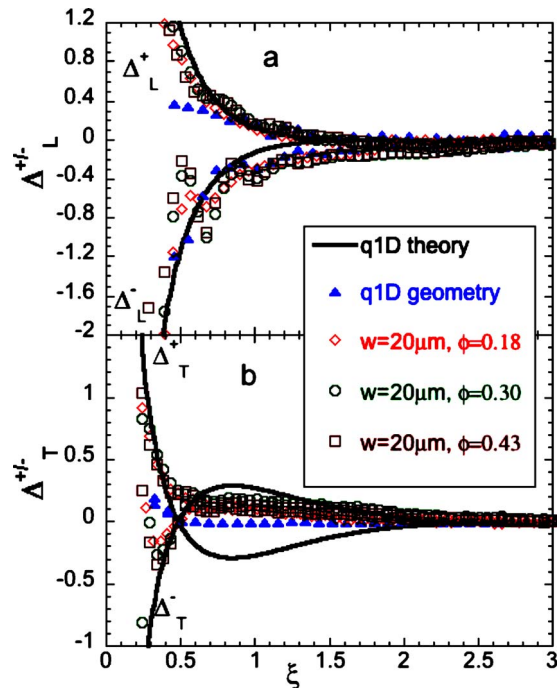


FIG. 12. (Color online) Reduced pseudo-q2D (a) longitudinal and (b) transverse pair-diffusion coefficients  $\Delta_{L,T}^{\pm}$  at the higher packing fraction for the particles in the inner strata of a ribbon channel ( $w=20 \mu\text{m}$ ), scaled by a factor  $R$  ( $5 \leq R \leq 8 \mu\text{m}$ ). Also displayed are  $\Delta_{L,T}^{\pm}$  for the q1D fluid at  $\eta=0.17$  [3]. The lines are the predicted  $\Delta_{L,T}^{\pm}$  from the Stokeslet hydrodynamic analysis for a q1D geometry [14].

a universal curve are much larger than  $H$  used for  $r \leq w$ ; for  $\Delta_L^{\pm}$ ,  $R \approx 6, 8, 8, 8, \text{ and } 6 \mu\text{m}$ , corresponding to  $w=5, 8, 11, 14, \text{ and } 20 \mu\text{m}$ , respectively, and for  $\Delta_T^{\pm}$ ,  $R \approx 5, 6, 7, 7, \text{ and } 7 \mu\text{m}$ , corresponding to the same set of  $w$ 's. Figure 12

shows the typical density-independent behavior of the pseudo-q2D  $\Delta_{L,T}^{\pm}$  in one of the ribbon channels ( $w=20 \mu\text{m}$ ) at different packing fractions, and the same sets of  $R$  values are used for all the packing fractions. The agreement between the pseudo-q2D  $\Delta_{L,T}^{\pm}$  and the predicted q1D  $\Delta_{L,T}^{\pm}$  indicates clearly that when  $r \gg w$  the ribbon channels do act as q1D capillaries for the confined particles, even though the particles are not in single files.

#### IV. CONCLUSION

In summary, the resulting picture emerging from our measurements is surprising in its richness. In particular, the answers to the questions posed in the beginning of this paper are found to be multifaceted; while certain dynamic properties of the confined suspensions exhibit q2D characteristics already for relatively narrow channels, other properties continue to significantly deviate from the expected q2D behavior even for the widest channels studied. We conclude that the transition between q1D and q2D behaviors is apparent to different extent in different system properties. Contrary to widely held opinion, the transition in system properties is not complete until the width of the confined ribbon is considerably greater than the largest we have studied.

#### ACKNOWLEDGMENTS

The research reported in this work was supported by the NSF supported MRSEC Laboratory (Contract No. DMR-0820054) at the University of Chicago, and the Israel Science Foundation (Contract No. 588/06). B.L. is grateful for the support of ChemMatCARS, which is funded by NSF-CHE, NSF-DMR, and the DOE-BES (Contract No. NSF/CHE-0822838).

- [1] H. Diamant, *J. Phys. Soc. Jpn.* **78**, 041002 (2009).
- [2] B. Cui, H. Diamant, B. Lin, and S. A. Rice, *Phys. Rev. Lett.* **92**, 258301 (2004).
- [3] B. Cui, H. Diamant, and B. Lin, *Phys. Rev. Lett.* **89**, 188302 (2002).
- [4] C. Bechinger, *Curr. Opin. Colloid Interface Sci.* **7**, 204 (2002).
- [5] J. Santana-Solano, A. Ramirez-Saito, and J. L. Arauz-Lara, *Phys. Rev. Lett.* **95**, 198301 (2005).
- [6] X. Xu, S. A. Rice, B. Lin, and H. Diamant, *Phys. Rev. Lett.* **95**, 158301 (2005).
- [7] T. Beatus, R. Bar-Ziv, and T. Tlusty, *Phys. Rev. Lett.* **99**, 124502 (2007).
- [8] V. Prasad, S. A. Koehler, and E. R. Weeks, *Phys. Rev. Lett.* **97**, 176001 (2006).
- [9] V. Prasad and E. R. Weeks, *Phys. Rev. Lett.* **102**, 178302 (2009).
- [10] C. R. Nugent, K. V. Edmond, H. N. Patel, and E. R. Weeks, *Phys. Rev. Lett.* **99**, 025702 (2007).
- [11] E. R. Dufresne, T. M. Squires, M. P. Brenner, and D. G. Grier, *Phys. Rev. Lett.* **85**, 3317 (2000).
- [12] D. Frydel and H. Diamant, *Phys. Rev. Lett.* **104**, 248302 (2010).
- [13] J. C. Crocker, *J. Chem. Phys.* **106**, 2837 (1997).
- [14] N. Liron and R. Shahar, *J. Fluid Mech.* **86**, 727 (1978).
- [15] N. Liron and S. Mochon, *J. Eng. Math.* **10**, 287 (1976).
- [16] K. W. Desmond and E. R. Weeks, *Phys. Rev. E* **80**, 051305 (2009).
- [17] D. Chaudhuri and S. Sengupta, *J. Chem. Phys.* **128**, 194702 (2008).
- [18] T. R. Stratton, S. Novikov, R. Qato, S. Villarreal, B. Cui, S. A. Rice, and B. Lin, *Phys. Rev. E* **79**, 031406 (2009).
- [19] B. Lin, B. Cui, J.-H. Lee, and J. Yu, *EPL* **57**, 724 (2002).
- [20] B. Cui, B. Lin, and S. A. Rice, *J. Chem. Phys.* **116**, 3119 (2002).
- [21] J. C. Crocker and D. G. Grier, *J. Colloid Interface Sci.* **179**, 298 (1996).
- [22] J. Happel and H. Brenner, *Low Reynolds Number Hydrodynamics* (Kluwer Academic, Dordrecht, 1983).
- [23] H. Diamant, B. Cui, B. Lin, and S. A. Rice, *J. Phys.: Condens. Matter* **17**, S4047 (2005).